2

Modeling Mother Rotor Anchoring in Branching Atrial Tissue*

Gerald Fischer[1], Leonhard Wieser[1] and Florian Hintringer[2,†]
[1]*Institute of Electrical, Electronic and Bioengineering, University for Health Sciences, Medical Informatics and Technology (UMIT), Hall i.T.*
[2]*Department for Cardiology, Medical University Innsbruck*
Austria

1. Introduction

Background: It has been hypothesized that stable mother rotors may increase the stability of atrial fibrillation. Local shortening of action potential duration due to vagotonic activity may promote the formation of mother rotors. However, prior studies have shown that meandering rotors typically drift out of the region of short action potential duration (APD), making the formation of stable rotors unlikely. Thus, for the formation of mother rotors in vagotonic AF a mechanism must be involved which increases rotor stability.
Hypothesis: Local variation of electrotonic load due to branching muscle sleeves in the atrial tissue may avoid rotor drift and ease the formation of stable vagotonic AF. In this chapter the underlying mechanisms are illustrated by means of computer modeling.
Model formulation: Anchoring is illustrated in a square patch of tissue and a monolayer model of the atria. Vagotonic activity was modeled by increasing ACh-concentration in the vicinity of the pulmonary veins (PVs). Close to the right lower PV, a muscle sleeve branching into the vein was included in the model. A model of canine atrial membrane kinetics was used providing detailed data on electrical remodeling and vagal activity. AF was analyzed computing dominant frequency (DF) maps and phase singularities (PSs).
Model predictions: In the case of a missing anchor site AF was self terminating within 2 s of simulated activity. The rotor drifted out of the short APD region. After including a branching tissue structure, mother rotor formation was observed (anchoring and almost periodic activity over the entire simulated interval of 4.2 s). Pull and push currents were identified as the mechanism stabilizing the rotor trajectory. Push currents in the bundle reduced the DF at the branching by about 10% with respect to the highest DF (15 Hz). The computed DF map mainly reflected the underlying ACh concentration (correlation 0.9).
Summary: Branching tissue structures in regions of high ACh-concentration may constitute the substrate underlying vagotonic AF. Future experimental studies are needed to further confirm motor rotor anchoring in branching tissue.

*Research on cardiac arrhythmia is supported by the Standortagentur Tyrol within the K-Regio Projekt Kryotipkatheter.
†Disclosures: G. Fischer and F. Hintringer are partners at AFreeze GmbH.

2. Background

Several mechanisms are involved in the onset and the maintenance of atrial fibrillation (AF), Nattel (2002). Beside the conceptual models of multiple self-maintaining wavelets and fast firing ectopic foci, also mother rotors have become subject of basic and applied research. A mother rotor is thought to be a locally very organized and fast micro-reentry circuit driving AF. While the original concept of a single driving reentry underlying AF goes back to the early twentieth century, high resolution optical mapping, Chen et al. (2000) and micro-electrode recordings, Mandapati et al. (2000) in the Langendorff-perfused sheep heart led to an increased interest in mother rotors in this century. Recently, electro-anatomical mapping displayed regions of high dominant frequency (DF) in humans, Sanders et al. (2005). Several DF sites were found per patient.

In computer models of atrial and ventricular fibrillation mother rotors are associated with regions of local shortening of the action potential duration (APD), Samie et al. (2001). Such shortening is obtained by heterogeneous membrane properties which can arise for instance from a locally increased concentration of the vagal neurotransmitter acetylcholine (ACh), Kneller et al. (2002). However, a single region of short APD does not guarantee the formation of a mother rotor. Any heterogeneity in membrane properties causes a rotor or spiral wave drift. As has been shown by Ten Tusscher & Panfilov (2002), the rotor typically tends to drift towards regions of long APD. This hampers the formation of mother rotors. In Kneller et al. (2002) a multiple number of properly sized ACh-regions was needed for creating a stable rotor of high frequency.

3. Hypothesis

The central hypothesis of this chapter is to illuminate a mechanism which reverses the direction of rotor drift and, thus, supports anchoring of mother rotors. The anchor site is formed by a branching tissue structure in the region of short APD. There are multiple branchings in the atria such as inter-atrial connections (e.g., the Bachmann's bundle [BB]), muscle sleeves branching from the left atrium into the pulmonary veins (PVs), the pectinate muscles, etc. Normal conduction in branching tissue is well investigated, Fast & Kléber (1995), Kucera & Rudy (2001). If a wavefront activates a bundle an increased current is drawn by the increased load of the branching tissue. This causes slowing of conduction or even functional block. Kucera and Rudy named this the pull-effect. Once the bundle is activated, current is re-injected back into the branching bringing the cells burdened by the pull currents back to a normal plateau level. This effect reduces the window of vulnerability and is named the push effect. For fibrillatory conduction it has been shown that a branching can create wave breaks but also an anchor site and that pull and push currents are involved in these phenomena, Wieser et al. (2007).

The hypothesis was tested as follows: first, a square patch of tissue was investigated for demonstrating rotor drift out of the ACh-region in the absence of an anchor site. This lead to spontaneous termination of fibrillation. The same finding was obtained for a model of the atrial geometry. Second, an anchor point was included in the ACh-region of the square patch by a branching tissue structure. It was shown that the direction of drift is reversed and a mother rotor was formed. Also, for the model of atrial geometry an anchor site increased the rotor stability.

4. Model formulation

4.1 Bioelectric activity

The membrane kinetics were described by the ionic current model of the atrial canine cell developed by Ramirez et al. (2000). As described in Xie et al. (2002) Na^+ and Cl^- concentrations were set to a fixed predefined value. Vagal actions were included by the acetylcholine (ACh) sensitive K^+-current as formulated by Kneller et al. (2002). Heterogeneous membrane properties were introduced into the models by spatially varying the ACh concentration. An adaptive time step scheme was used for solving the ordinary differential equations, Wieser et al. (2007).

Cell to cell coupling in atrial tissue was described by the monodomain equation. The finite element method was used for spatial discretization. The approximate edge length of a cell element was 200 μm. Time integration of the monodomain equation was performed using an explicit Euler scheme, treating the ionic current part and the diffusion part separately. Further details can be found in Wieser et al. (2007). Tissue properties were described by the following parameters: surface to volume ratio of the cell (100 mm^{-1}), cell capacitance per unit area (0.01 μFmm^{-2}) and conductivity (values given below).

Fibrillatory conduction was simulated for a time interval of 4.2 s duration. This interval is identical as for the recorded data in Sanders et al. (2005) and Fischer et al. (2007).

4.2 Square model

A $60 \times 60 \times 1$ mm^3 block of cardiac tissue including a bundle of cylindrical shape (diameter 3 mm) in the tissue center was constructed. Fibers were included within the bundle running along its axis (longitudinal and transversal conductivity are 0.3 S/m and 0.1 S/m, respectively). For the rest of the tissue an isotropic conductivity of 0.1 S/m was assumed. This yields a propagation velocity of about 47 cm/s in the bulk tissue and a velocity of about 83 cm/s along the bundle. In order to study the effective role of the bundle in the simulations it was also possible to remove the bundle from the model. An ACh concentration was assigned to a circular region (diameter 50 mm) centered at the tissue center (i.e. the bundle insertion). Here, the maximal ACh concentration was 0.003 μM. Similar as in Kneller et al. (2002), a harmonic function was used for assigning a smooth transition of the concentration to zero (no ACh outside the region). Electrical remodeling was considered by reducing the Ca^{2+} current to 20% of its original value.

4.3 Atrial model

A detailed description of our atrial model and the model validation for sinus rhythm and paced beats can be found in Wieser, Richter, Plank, Pfeifer, Tilg, Nowak & Fischer (2008). Briefly, a monolayer representation of the atria (curved surfaces in space) was created based on magnetic resonance (MR) imaging data of a female patient (50 kg body weight) with a supraventricular arrhythmia but a structurally normal atrium, Berger et al. (2006). The left and the right atrium (LA, RA, resp.) are electrically connected via three conductive structures: Bachmann's bundle (BB), a coronary sinus (CS) muscle sleeve and the rim of the fossa ovalis (FO). In the monolayer representation BB and the CS muscle sleeve are strip-like structures with insertions in either atrium. The FO itself is non-conductive except for the rim. Thus, it is represented as a hole in the atrial septum. A ring-like structure represents the conducting rim and connects the FO orifices to each of the atria.

The atrial monodomain conductivity was assumed to be isotropic with 0.08 S/m (reference value). For all fibrous structures in the model (BB, CS muscle sleeve, crista terminalis) the longitudinal conductivity was increased to a 3–6 fold of the reference. The transversal conductivity is identical to the reference (0.08 S/m). For the FO (poor conduction) one fourth

of the reference conductivity was chosen. The conduction velocity obtained by the reference conductivity was 43 cm/s. The maximum diameter of the atrial geometry was 3.8 cm [RA] and 4.3 cm [LA].
Atrial remodeling was considered by reducing the Ca^{2+} current to 31% and the fast transient outward K^{+}-current to 35% of the original value. According to experimental data for the normal and remodeled canine atrial cell, Ramirez et al. (2000), this corresponds to a degree of electrical remodeling obtained after 42 days of persistent atrial tachycardia. The ACh concentration was increased around the PVs as vagal nerve endings can be found in this region Armour et al. (1997). From the MR data only one common left pulmonary vein (LPV) ostium was identified. In a circular region around each ostium the ACh concentration was interpolated by a harmonic function. The maximal concentration was 0.02 μM. The diameters of the three ACh-regions were 50 mm. In the area between the two right PVs the regions were overlapping in part. Here, the higher of the two concentration values was taken.
For our study an anchoring bundle could be introduced close to the right lower PV. The bundle was mimicking a muscle sleeve extending into the PV. Due to the monolayer representation of the atrium the bundle had a strip like structure with a width of 2 mm. The bundle branched off from the atrial tissue about 4 mm peri-ostial from the PV. Its longitudinal conductivity was the six-fold of the reference conductivity while the transversal conductivity was equal to the reference.

4.4 Phase information and dominant frequency

Phase information is computed as described in Iyer & Gray (2001) using two independent variables of each cell, namely the action potential V (reference value -40 mV) and the h-gate (sodium inactivation gate, reference value 0.4). On the triangulated atrial geometry phase singularities (PSs) are determined by applying the concept of topological charge as described in Rantner et al. (2007).
The direct current (dc) component was removed from the action potential prior to spectral analysis. This has a similar effect as appling a high pass filter component in clinicaly recorded data and enables the comparision of the spectral analysis with the the data shown in Sanders et al. (2005), Fischer et al. (2007). Furthermore, the data was was down-sampled to 250 Hz. Two different spectral estimators were used for computing the spectral profile of the action potential. First, the Fast Fourier Transform (FFT) was used which is a kind of standard for computing dominant frequency (DF), Kneller et al. (2002), Sanders et al. (2005), Fischer et al. (2007). For the simulated time interval of 4.2 s the obtained frequency resolution is 0.24 Hz. Second, a spectral estimator based on autoregressive (AR) modeling (Yule-Walker method), Signorini et al. (2003) was used for improving the spectral resolution. The Yule-Walker method performs well if the spectrum is expected to contain pronounced peaks. However, this spectral estimator looses accuracy if the sampling frequency is too high. Thus, a two point moving average low-pass filter was applied and the sampling frequency was halved to 125 Hz (about the ten-fold of the expected DFs). The AR-model order was fixed to twelve, which means that not more than six prominent peaks are expected to appear in the spectral profile. The spectrum was computed with a resolution of 0.01 Hz and the maximum of the power spectral density was taken as the DF.
Action potential data and phase singularities were continuously displayed for all computer simulations with a temporal resolution of 1 ms as described in Rantner et al. (2007) using the computer visualization package AmiraDev 2.3. Note that each PS is automatically detected by the computer program and directly linked to statistical evaluation removing any observer depended bypass. Furthermore, also the DF maps have been displayed with AmiraDev 2.3 and computer supported detection of low and high sites.

5. Model predictions

5.1 Missing anchor

A spiral wave was initiated in the square model with its tip close to the tissue center. First, the bundle was removed (missing anchor site). Within the first second of simulated activity the spiral wave formed a meandering rotor. A DF of 12.5 Hz (FFT) was obtained in the region of high ACh concentration (short APD). Outside this region the tissue could not follow the rapid activation and wave breaks gave rise to chaotic activity at a lower DF (8.5 Hz). In total 28 new phase singularities were generated with a relatively short life span (3 ms to 759 ms, mean 128 ms). As expected, the original rotor was slowly drifting out of the region of short APD and terminated after 1314 ms by a collision with a PS of opposite chirality. After 1866 ms fibrillation terminated spontaneously by the collision of the last two PSs.

A similar behavior was observed for the atrial geometry in the absence of an anchor site. The APD was shortened in the proximity of the pulmonary veins by an increased ACh concentration. Fibrillation was induced by cross shock protocol. Two PSs were created by a wave break in the region of short APD close to the right lower pulmonary vein. Similar as in the square model, one PS became a rotor of a long life time meandering with a slow drift towards regions of longer APD. After 932 ms it died out by collision (see Fig. 1). Again, wave breaks occurred in the border zone of the short APD regions. Furthermore, wave breaks were observed at the left atrial insertion of the Bachmann's bundle due to load effects in branching tissue. In total 125 PSs of relatively short life time (4 ms to 468 ms, mean 60 ms) were counted. Again fibrillation terminated spontaneously after 1528 ms by collision of the last PS with border of the anterior lateral mitral annulus.

5.2 Mechanism of anchoring

Again, a spiral wave was initiated in the square model with its tip close to the center. This time, the bundle was included in the model. Thus, APD was prolonged at the branching site due to the push currents drawn in the plateau phase. This effect locally reversed the APD gradient produced by the acetylcholine distribution. Thus, the meandering spiral wave tip displayed a slow drift towards the bundle. After 220 ms, the rotor attached to the bundle for the first time and then displayed a repeatable activation pattern.

One cycle (one full PS rotation) of the repeatable activation pattern is shown in Fig. 2. At 300 ms the PS reached the bundle in an eleven o'clock position. Due to the push currents of the previous cycle the cells in the branching were not yet recovered. Thus, the rotor was forced to circumvent the bundle along its right border. Strong pull currents were drawn from the area right to the bundle, as the activation front traveled close to an increased and unexcitable load (refractory tissue branching). The bundle became conductive when the rotor reached a six o'clock position (321 ms). Now the excitable region was inside the bundle and the refractory tissue was outside the right border (due to the strong pull currents the tissue had already recovered to about -65 mV). The rotor traveled the same way back along the border and detached again in an eleven o'clock position (folding of the trajectory). Due to the small area of the excitable gap the rotor was accelerated when traveling back (traveling down takes about 20 ms, while traveling back up takes only 10 ms). As the rotor was drifting away from the bundle the push currents prolonged the plateau phase in the bundle. At 345 ms it can be clearly seen in the color coding that the action potential within the bundle was higher ('push region') than within the right vicinity of the bundle ('pull region'). Then the rotor meandered back towards the bundle (360 ms). The pull region recovered first and attracted the rotor. Thus, the rotor moved again towards the right bundle border where the strongest pull currents were observed. This time the bundle was reached in a twelve o'clock position. The cycle was then repeated which a pattern slightly rotated in a clockwise fashion. Due to this slight

rotation in each cycle a rosette like trajectory of the rotor is obtained for the entire simulated time interval of 4.2 s.
Within the bundle region the DF was 11.3 Hz (FFT). Interestingly, the DF in the surrounding of the bundle was somewhat increased with a value of 12.3 Hz. Outside the ACh region the DF ranged from 8.0 Hz to 8.5 Hz. The mother rotor persisted for the entire simulated time. The remaining 117 PSs had a short life span (6 ms to 296 ms, mean 46 ms) and were all created by wave breaks.

5.3 Mother rotor in the atrium

A bundle was included close to the right lower pulmonary vein of the atrial geometry. Fibrillation was induced as before by a cross shock protocol applied close to the bundle. Two phase singularities were created by a wave break and the one closer to the bundle drifted in a meandering fashion towards the bundle and reached the bundle 4 ms after its initiation for the first time. It detached again, and after three rotations taking another 212 ms it anchored again. Then, similar as in the square model, it attached and detached repeatedly forming a mother rotor which lasted for the entire simulated time interval (4.2 s). The rotor trajectory is shown in Fig. 3 together with a the action potential in a cell near the bundle (mother rotor area) and the spectra obtained by the FFT and the AR-model.
The remaining 744 PSs were of relatively short life span (4 ms to 536 ms, mean 45 ms). The majority was created in the border zones of the acetylcholine areas near the PVs. Furthermore, frequent wave breaks were observed at the left atrial insertion of the Bachmann's bundle (increased load at the tissue branching). To a smaller degree wave breaks were also observed at the right atrial insertion of the Bachmann's bundle and at the two connections of the coronary sinus muscle sleeve with both atria. Also unstable anchoring of PSs at the Bachmann's Bundle was observed. As there is no acetylcholine (long APD) in this region no stable rotor was formed. Typically, the PSs attached only once or twice at the Bachmann's bundle and died out in the meandering phase when traveling away from the bundle by collision with other PSs. Only 122 PSs (16%) were observed in the right atrium. Figure 4 shows three sample snapshots of chaotic conduction in a left anterior oblique view.
The dominant frequency map was computed by the FFT and the AR-model. Some results are listed in Tab. 1. The DF map obtained for the AR-model is shown in Fig. 5. For all cell elements the correlation between the two spectral estimators is 0.97. Similar as for the square model the highest frequency (15.4 Hz, AR) is obtained in the tissue surrounding the bundle. Again in the bundle itself the frequency is slightly reduced (13.8 Hz, AR). Here, comparisons are based on AR-model data due to the better spectral resolution.
Interestingly, also at the common left pulmonary vein (14.9 Hz) a higher DF is obtained than at the bundle itself. As can been from Fig. 5, the DF distribution closely matched the ACh concentration. The DF map shows a high correlation with the ACh concentration (0.89 FFT, 0.90 AR-model). The lowest DF in the left atrium is found at the left atrial appendage (6.4 Hz). In the right atrium the DF is almost constant (6.5 Hz to 7.2 Hz). The transition from high DF regions (blue) to low DF regions (red) occurs in a narrow region. Note the effect of the Bachmann's bundle on the left atrial DF map in Fig. 5. The low frequency region in the basal anterior left atrium extends up to the bundle insertion. This can be explained by push currents prolonging the APD in the tissue branching.

6. Summary

6.1 Anchoring

The major scope of this study was the investigation of load effects fixing a mother rotor pathway in a region of short APD. Before anchoring, the push currents prolong the APD at the

branching. Thus, a spiral wave in the vicinity drifts towards the bundle and anchors. Strong pull currents are drawn by the large unexcitable load (refractory bundle). When the bundle becomes excitable, the phase singularity travels back. Within the bundle the push currents prolong the APD (push region). This is a major difference to normal conduction where the pull currents drawn from a cell are later injected back by push currents into the same cell.
It has been shown previously by Wieser et al. (2007) that for a rectangular patch of tissue with homogeneous membrane properties anchoring is mainly determined by the load of the branching structure. Varying the shape of the bundle the rotor trajectory changes too, but the basic effect that the trajectory is fixed at the bundle is still observable. Even for the idealized situation of a flat strip in the monolayer model anchoring takes place. Several effects stabilize the rotor. First, the interaction of pull and push currents cause a folding of the trajectory at the bundle border. This lengthens the rotor pathway. Second, in the pull phase (wavelet outside the bundle) the strong load decreases the speed of the rotor. This contributes to a short wavelength. Third, the pull currents produce a zone which recovers early and attracts the rotor.
Interestingly, the interaction of APD prolongation in the bundle (push effect) and folding of the rotor trajectory makes it possible that the DF at the anchor site is somewhat below the DF of the surrounding tissue. At this point its should be stressed that the slight local decrease in DF (around 10%) is biophysically reasonable as push currents prolong the APD in the branching. Furthermore, the slight local decrease in DF was confirmed by two independent spectral estimators (FFT and AR-model). For the FFT the decrease was only four digits of the spectral resolution (1 Hz). Thus, a second spectral estimator (AR-model) with a theoretically infinite spectral resolution (but still a limited accuracy) was used. With this method a continuous decrease of DF was observed when zooming into the region around the bundle (data not shown). To our experience the AR-model is more accurate than the FFT for stationary signals (no termination of AF in the investigated time interval).
It must be stressed that permanent anchoring needs both local APD shortening and a branching tissue structure. Short time anchoring was observed at the left atrial insertion of the BB. Due to the long APD in this region the rotor was forced to travel far away from the bundle when detaching. This provoked a collision with PSs originating from the ACh-border zone. Another effect frequently observed in branching tissue is a wave break (Fig. 4) caused by the transition of an intact wave front, Wieser et al. (2007).

6.2 Left atrial AF

Induction of AF by a cross shock near one of the PVs can be interpreted as a critically timed extrasystole originating from a pulmonary vein. One of the two created PSs anchored within 0.2 s and became the mother rotor. Also within 0.2 s the first wave breaks occurred at the border of the ACh-region creating a completely chaotic activation pattern for large parts of the left atrium. In the right atrium the first PSs were observed 1.3 s after induction of AF. They were created by a wave break caused by the irregular stimuli across the interatrial connections in combination with steep restitution curve of the right atrial cells, Virag et al. (2002). Wave breaks at the right atrial insertions of the interatrial connections (BB, CS, FO) created PSs of only a few milliseconds life span. In the left atrium the number of PSs counted was the five-fold compared to the right atrium.
For the constructed model (the anchor site and the ACh-regions are near to the PVs) AF is a left atrial disease. We do not claim that this is true for all types of AF. However, it is an interesting observation that reasonable assumptions can be made (muscle sleeves and ACh-regions close to the PVs) which make the left atrium the source and the right atrium the innocent bystander.

6.3 Clinical implications

In the past decade catheter ablation of AF was mainly focusing on the left atrium and here in particular on the ostia of the PVs, Cappato et al. (2005). Originally, the attention paid to the anatomical structure of the PVs was motivated by a report identifying muscle sleeves from the PVs as triggers of AF, Haïssaguerre et al. (1998). To a smaller degree also other left and right atrial structures can host triggers. In the performed computer simulations a muscle sleeve branching from the atrial muscle could also constitute the substrate of the arrhythmia.

From a clinical point of view the understanding of paroxysmal AF is dominated by the picture of rapidly firing foci triggering the onset of the arrhythmia. Interestingly, the results of the presented computer model and other simulation studies, Wieser, Nowak, Tilg & Fischer (2008), Kneller et al. (2002), Kneller et al. (2005) suggest that fibrillation terminates within very few seconds without additional involved stabilizing mechanisms. For the investigated model of vagotonic AF the interplay of electrical remodeling, vagotonic activity and conduction in branching tissue structures stabilizes the reentry pathway. They constitute, thus, the substrate of the arrhythmia. This enables the development of longer, haemodynamically relevant episodes of AF. Thus, muscle fibers branching from the left atrium into the PVs do not only constitute the triggers of paroxysmal AF but may form also its substrate. In the computer model AF terminates within less than two seconds when removing the bundle from the vein. Similarly, AF often terminates during catheter ablation due to a modification of the underlying substrate. Here, future experimental work is needed for confirming the predictions of the computer model.

Guided ablation of AF needs signal parameters which identify the maintaining substrate(s). Here, two signal types are considered marking potential ablation targets: high DF sites, Sanders et al. (2005) and locations with fractionated potentials, Rostock et al. (2006).

It has been shown for patients with paroxysmal AF that ablation at a high DF site can terminate AF, Sanders et al. (2005). In our computer model the anchor site did not display the highest DF but a slightly reduced value (in the order of the spectral resolution obtained by the FFT). This discrepancy could be explained by keeping in mind that different signal types are used in clinical routine and computer modeling. A computer model yields the action potential (containing the intracellular potential) with a submillimeter spacial resolution. In contrast to this, mainly bipolar electrocardiograms (extracellular potentials) are assessed during an electrophysiological study. For the typical electrode spacing in the order of a few millimeters the catheter signal is sensitive to electric activity in a patch of tissue with several millimeters of diameter. Thus, the limited spatial and spectral resolution of current clinical technology can easily mask the small local decrease of DF predicted by our model.

The DF map computed by our computer model closely approximates the ACh-distribution in the atrial model (correlation coefficient 0.9). Branching tissue structures like the left atrial BB insertion and the PV muscle sleeve have only a minor influence on the DF map. It appears that the DF map in our model gives primely a picture of ACh-concentration. Also at the PVs without an anchor structure the computed DF was high. Interestingly, the computed DF map is in good qualitative agreement (high DF near the PVs, low DF in the right atrium and the basal anterior left atrium) with the DF map shown in Sanders et al. (2005) for paroxysmal AF. One might speculate that for paroxysmal AF the DF map displays mainly a picture of the vagal tonus.

6.4 Model simplifications

Every model is per definition a simplified and abstract approximation of a true system. The developed model is no exception from this rule.

The actual size and dimensions of the included branchings are not based on detailed anatomical data. They were assumed in the range of a few millimeters Wieser et al. (2007).

	FFT	AR-model
	Hz	Hz
maximum left atrium	15.5	15.4
minimum left atrium	6.0	6.4
maximum right atrium	7.9	7.2
minimum right atrium	6.0	6.5
mean of both atria	9.9	9.4
anchor site	14.3	13.8
left pulmonary vein	15.2	14.9

Table 1. Dominant Frequency computet by the FFT and AR-modeling

This seems reasonable for the largest muscle bundles in the atria. Also the distribution of ACh was assumed similarly as suggested in earlier computer models Kneller et al. (2002), Kneller et al. (2005) and in agreement with anatomical studies on atrial vagal innervation Armour et al. (1997). With the variation of these parameters also the strength of the observed rotor stabilization might change. However, the principal observation that tissue branchings in regions of short APD can contribute to mother rotor anchoring should remain valid. Having in mind that for example in the proximity of the PV ostia we find both, APD shortening and branching muscle fibers, the observed mechanisms could yield a contribution to mother rotor stabilization in humans.

We do not claim that the described mechanism of rotor stabilization is the sole or most important mechanism contributing to the formation of sustained AF. A plurality of other mechanisms is well investigated which contribute to stable AF. These mechanisms involve locally organized activity Kneller et al. (2005) but also entirely random activation which might be facilitated structural and mechanical remodeling Wijffels et al. (1995). The chapter presents a model of vagotonic AF based on reasonable assumptions.

We do also not claim that the stability observed for the short time span of a few seconds can be generalized to significantly longer periods of hour and days. However, it has been shown that the described mechanism can significantly prolong the live time of a fibrillatory episode. Thus, it might contribute to the formation of long periods of AF.

The atrial membrane kinetics were approximated by a computer model of the canine atrial cell. It was chosen as it contains detailed data for electrical remodeling by Ramirez et al. (2000) and vagal modulation of function Kneller et al. (2002). The atrial anatomy was human. The canine atrial cell has a relatively short APD Ramirez et al. (2000). This explains the relatively high DF (6 Hz to 15 Hz) predicted by our model. In humans the DF remains in the range of 4 Hz to 10 Hz in patients with paroxysmal AF. Sanders et al. (2005).

The use of a monolayer approximation of the atrium yields a significant save in computation time Wieser, Richter, Plank, Pfeifer, Tilg, Nowak & Fischer (2008), Virag et al. (2002), Vigmond et al. (2001). However, the variation of wall thickness cannot be included in the model. Furthermore, it has been shown that load effects are slightly over-estimated Wieser, Richter, Plank, Pfeifer, Tilg, Nowak & Fischer (2008). The predictions of the described model are consistent with a prior studies where bundle dimensions/geometry and ACh concentration have been varied, Wieser, Nowak, Tilg & Fischer (2008).

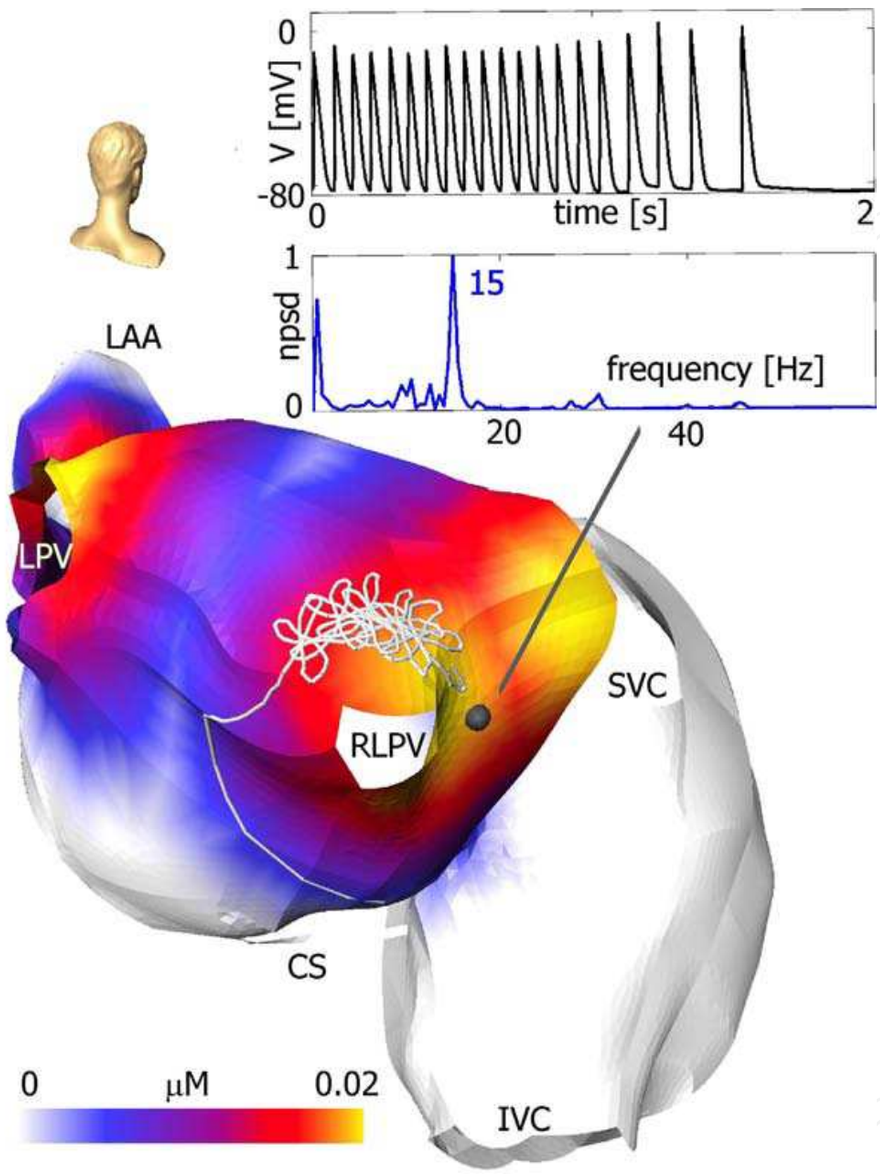

Fig. 1. Rotor drift in the case of a missing anchor site. The atrial model is shown in a posterior oblique view. Color coding displays the ACh concentration. The rotor trajectory is displayed by a white line. After its initiation near the RLPV the rotor drifts in a meandering fashion in direction of decreasing ACh level. Close to the border of the ACh region the drift accelerates and the rotor moves without meandering down to the posterior septal left atrium. Here it dies out by collision with a PS of opposite chirality. The action potential at one site (gray marker) near the RLPV is shown together with the computed power spectrum (FFT).
CS ... coronary sinus muscle sleeve, IVC ... inferior vena cava, LAA ... left atrial appendage, LPV ... left pulmonary vein, RLPV ... right lower pulmonary vein, SVC ... superior vena cava.

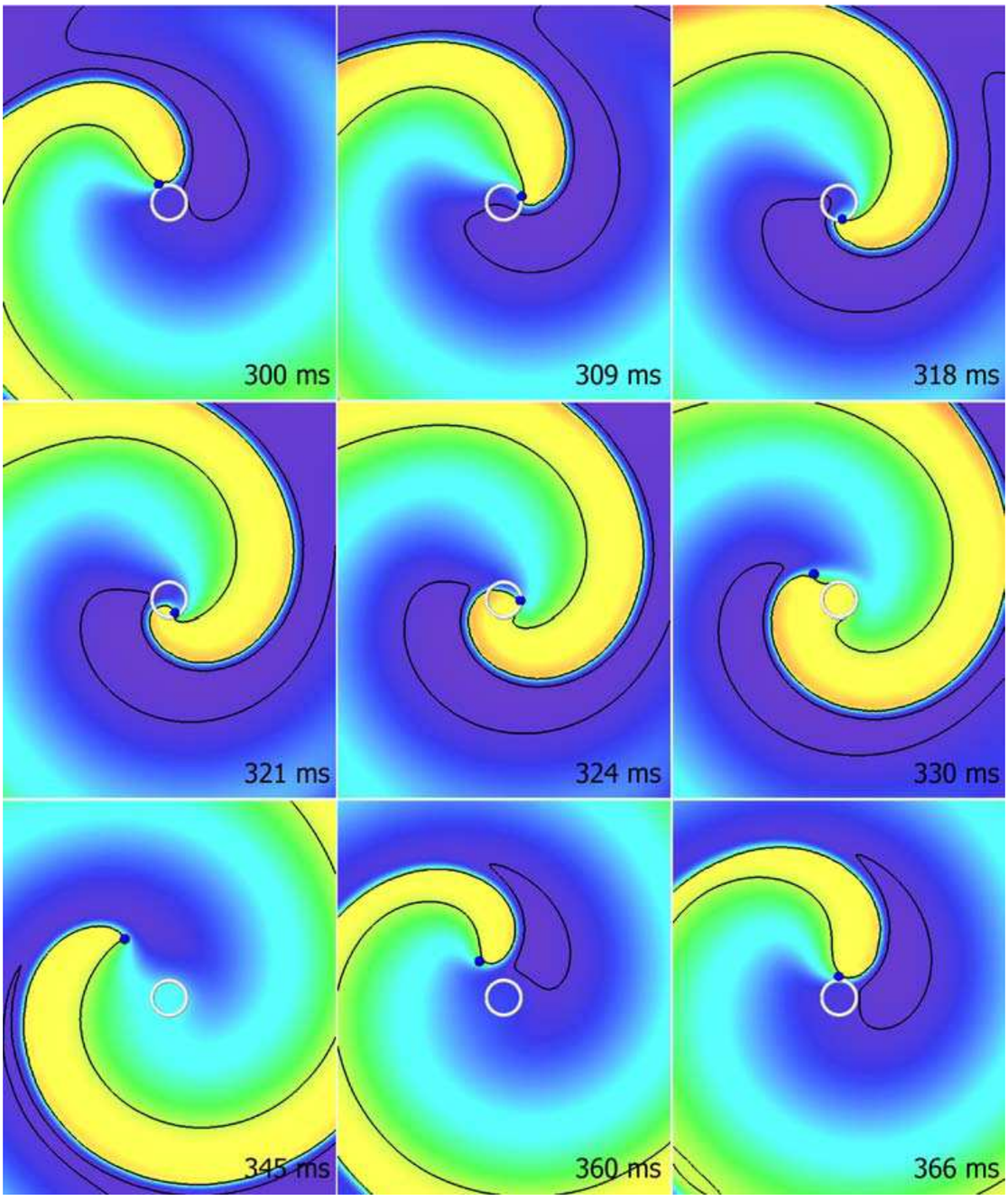

Fig. 2. One rotation of the anchored motor in the square model. Color coding depicts the action potential in the range of −80 mV (blue) to 0 mV(red). At t =300 ms the rotor (blue marker) has reached the bundle (white circle). The bundle region has not fully recovered yet and the activation front travels around its border (309 ms and 318 ms). Due to the potential gradient, pull currents are drawn from the wave front (area right from the bundle). At t =321 ms the bundle has recovered and the activation front can enter. Now the PS travels back along the bundle border as the excitable tissue is now inside the bundle (324 ms). When the PS has detached push currents increase the potential in the bundle prolonging APD (330 ms and 345 ms).

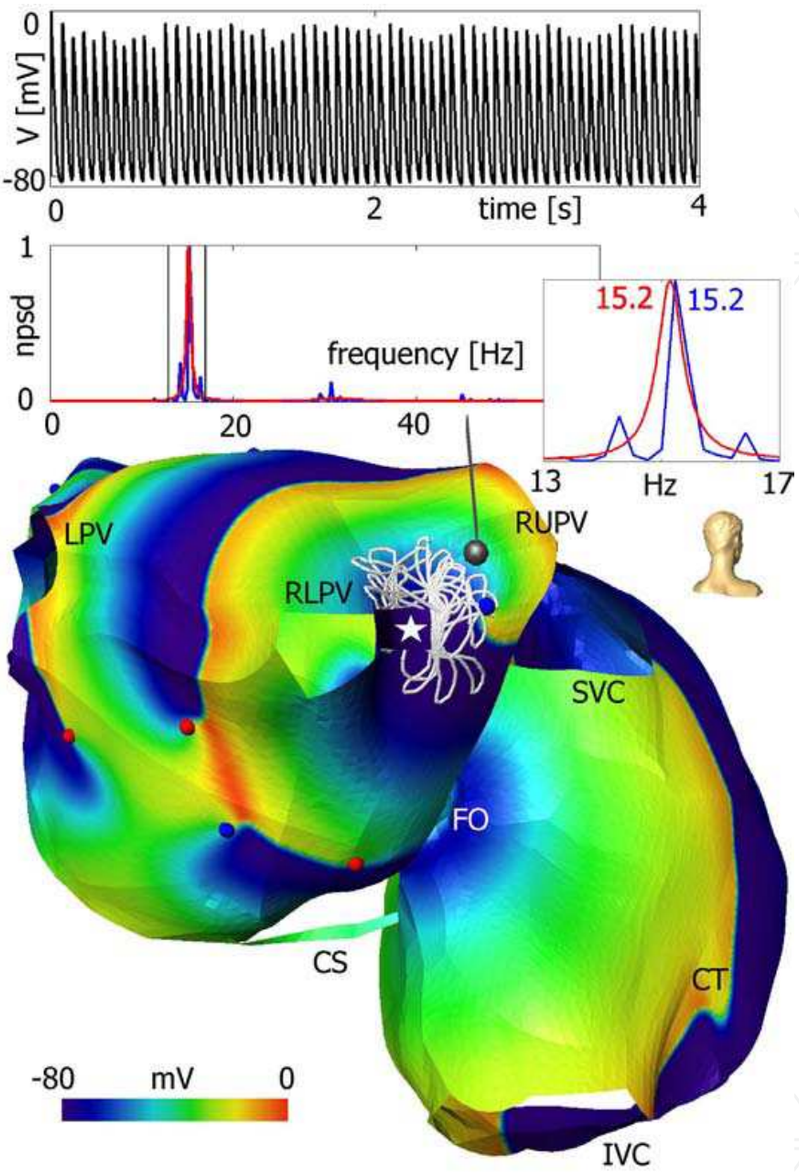

Fig. 3. Snapshot of the action potential after mother rotor anchoring. The atrial model is shown in a posterior oblique view. The mother rotor trajectory is displayed by a white line. Note meandering around the bundle insertion (white asterisk). Spherical markers represent PSs of clockwise (blue) and counter-clockwise (red) chirality. The action potential at a high frequency site (gray marker) is shown together with the power spectrum obtained by the FFT (blue) and the AR-model (red). A portion of the spectrum is zoomed for comparison.
CS ... coronary sinus muscle sleeve, CT ... crista terminalis, IVC ... inferior vena cava, FO ... fossa ovalis, LPV ... left pulmonary vein, RLPV ... right lower pulmonary vein, RUPV ... right upper pulmonary vein, SVC ... superior vena cava.

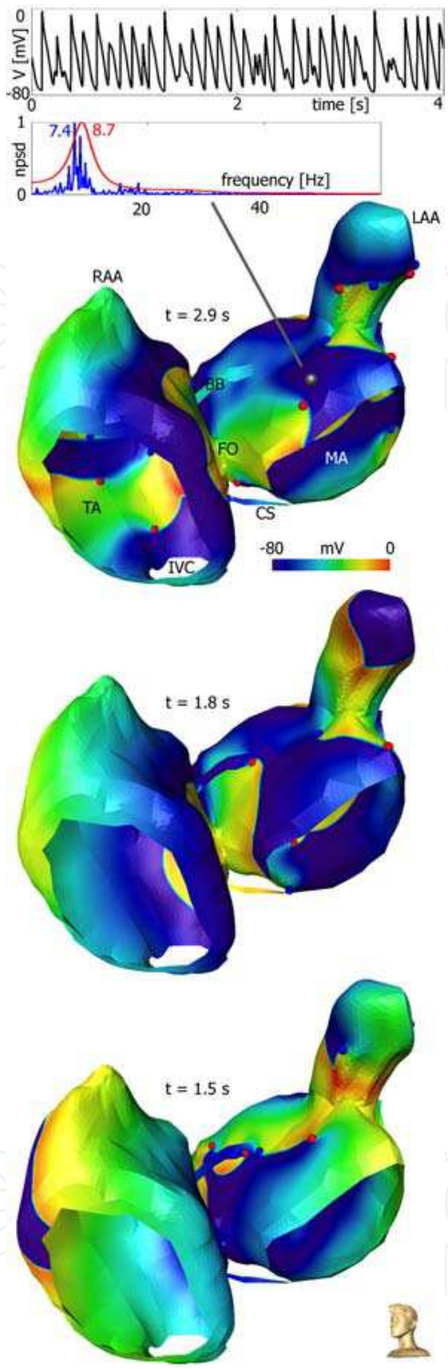

Fig. 4. Three snapshots of the action potential in a left anterior oblique view. On top the action potential in a low frequency site (gray marker) is shown together with the power spectrum. At 1.5 s a wave break can be observed at the left atrial insertion of the BB. At 1.8 s short time rotor anchoring takes place at the BB. Note that in general more PSs are on the left atrium compared to the right. Color coding and markers are the same as in Fig. 3.
BB ... Bachmann's bundle, CS ... coronary sinus muscle sleeve, FO ... fossa ovalis, IVC ... inferior vena cava, LAA ... left atrial appendage, MA ... mitral annulus, RAA ... right atrial appendage, TA ... tricuspid annulus.

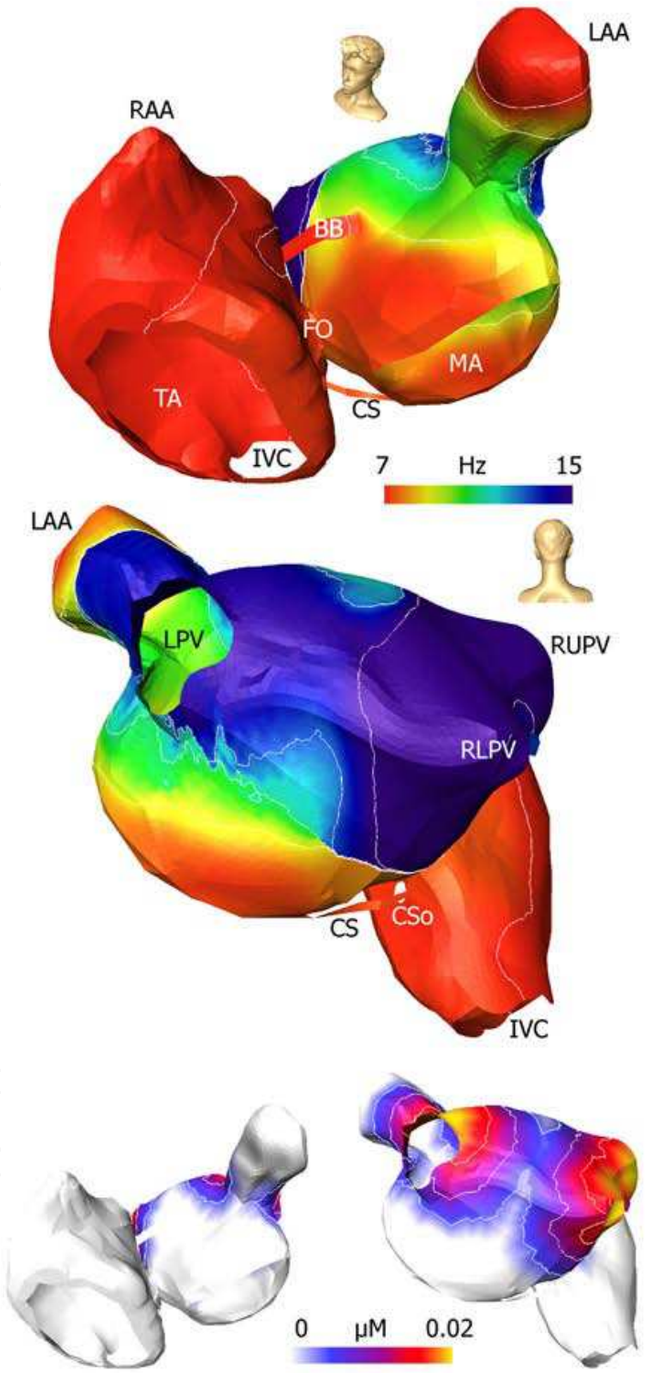

Fig. 5. Dominant frequency (DF) map computed by the AR-model. The upper panel shows the atrial model in a 45° left anterior oblique view. In the middle the atria are shown in a posterior view. Below the ACh-concentrations are shown for comparison.

6.5 Conclusions

A tissue branching (muscle sleeve, bundle, branching fibers) in a region of shortened action potential duration can serve as an anchor site for an organized activation pattern in vagotonic AF. The interplay of pull and push currents in the branching stabilizes the rotor pathway. The rotor repeatedly attaches and detaches. The locally short APD is necessary for maintaining the rotor. If APD prolongs (e.g., due to a reduced vagal tonus) the rotor can drift away from the anchor site and collide with another PS (possible spontaneous termination of AF).

Folding of the rotor trajectory and APD prolongation in the bundle (push currents) caused a modest decrease of DF at the anchor site. In our simulations the DF map was mainly influenced by the spatial distribution of acetylcholine. Thus, the DF map reflected the underlying assumed vagal activity.

7. References

Armour, J., Murphy, D., Yuan, B.-X., MacDonald, S. & Hopkins, D. (1997). Gross and microscopic anatomy of the human intrinsic cardiac nervous system, *The Anatomical Record* 247: 289–298.

Berger, T., Fischer, G., Pfeifer, B., Modre, R., Hanser, F., Th. Trieb, F. R., Stühlinger, M., Pachinger, O., Tilg, B. & Hintringer, F. (2006). Single-beat noninvasive imaging of cardiac electrophysiology (NICE) of ventricular preexcitation, *Journal of the American College of Cardiology* 48: 2045–2052.

Cappato, R., Calkins, H., Chen, S.-A., Davies, W., Iesaka, Y., Kalman, J., Kim, Y.-H., Klein, G., Packer, D. & Skanes, A. (2005). Worldwide survey on the methods, efficacy, and safety of catheter ablation for human atrial fibrillation, *Circulation* 111: 1100–1105.

Chen, J., Mandapati, R., Berenfeld, O., Skanes, A., Gray, R. & Jalife, J. (2000). Dynamics of wavelets and their role in atrial fibrillation in the isolated sheep heart, *Cardiovascular Research* 48: 220–232.

Fast, V. & Kléber, A. (1995). Cardiac tissue geometry as a determinant of unidirectional conduction block: assessment of microscopic excitation spread by optical mapping in patterned cell cultures and in a computer model, *Cardiovascular Research* 29: 697–707.

Fischer, G., Stühlinger, M., Nowak, C., Wieser, L., Tilg, B. & Hintringer, F. (2007). On computing dominant frequency from bipolar intracardiac electrogram, *IEEE Transactions on Biomedical Engineering* 54: 165–169.

Haïssaguerre, M., Jaïs, P., Shah, D., Takahashi, A., Hocini, M., Quiniou, G., Garrigue, S., Le Mouroux, A., Le Metayer, P. & Clementy, J. (1998). Spontaneous initiation of atrial fibrillation by ectopic beats originating in the pulmonary veis, *The New England Journal of Medicine* 339: 659–666.

Iyer, A. N. & Gray, R. A. (2001). An experimentalist's approach to accurate localization of phase singularities during reentry, *Annals of Biomedical Engineering* 29: 47–59.

Kneller, J., Kalifa, J., Zou, R., Zaitsev, A. V., Warren, M., Berenfeld, O., Vigmond, E. J., Leon, L. J., Nattel, S. & Jalife, J. (2005). Mechanisms of af termination by pure sodium channel blockade in an ionically-realistic mathematical model, *Circulation Research* 96: 35–47.

Kneller, J., Zou, R., Vigmond, E. J., Z.Wang, Leon, L. J. & Nattel, S. (2002). Cholinergic atrial fibrillation in a computer model of a two-dimensional sheet of canine atrial cells with realistic ionic properties, *Circulation Research* 90: e73–e87.

Kucera, J. & Rudy, Y. (2001). Mechanistic insights into very slow conduction in branching cardiac tissue: a model study, *Circulation Research* 89: 799–806.

Mandapati, R., Skanes, A., Chen, J., Berenfeld, O. & Jalife, J. (2000). Stable microreentrant sources as a mechanism of atrial fibrillation in the isolated sheep heart, *Circulation* 101: 194–199.

Nattel, S. (2002). New ideas about atrial fibrillation 50 years on, *Nature* 415: 219–226.

Ramirez, R., Nanttel, S. & Courtemanche, M. (2000). Mathematical analysis of canine atrial action potentials: rate, regional factors, and electrical remodeling, *American Journal of Physiology Heart Circulation Physiology* 279: H1767–H1785.

Rantner, L. J., Wieser, L., Stühlinger, M. C., Hintringer, F., Tilg, B. & Fischer, G. (2007). Detection of phase singularities in triangular meshes, *Methods of Information in Medicine* 46: 646–654.

Rostock, T., Rotter, M., Sanders, P., Takahashi, Y., Jaïs, P., Hocini, M., Hsu, L., Sacher, F., Clémenty, J. & Haïssaguerre, M. (2006). High-density activation mapping of fractionated electrograms in the atria of patients with paroxysmal atrial fibrillation, *Heart Rhythm* 3: 27–34.

Samie, F. H., Berenfeld, O., Anumonwo, J., Mironov, S. F., Udassi, S., Beaumont, J., Taffet, S., Pertsov, A. M. & Jalife, J. (2001). Rectification of the background potassium current – A determinant of rotor dynamics in ventricular fibrillation, *Circulation Research* 89: 1216–1223.

Sanders, P., Berenfeld, O., Hocini, M., Jaïs, P., Vaidyanathan, R., Hsu, L.-F., Garrigue, S., Takahashi, Y., Rotter, M., Sacher, F., Scavée, C., Ploutz-Snyder, R., Jalife, J. & Haïssaguerre, M. (2005). Spectral analysis identifies sites of high-frequency activity maintaining atrial fibrillation in humans, *Circulation* 112: 789–797.

Signorini, M., Magenes, G., Cerutti, S. & Arduini, D. (2003). Linear and nonlinear parameters for the analysis of fetal heart rate signal from cardiotocographic recordings, *IEEE Transactions on Biomedical Engineering* 50: 365–374.

Ten Tusscher, K. H. & Panfilov, A. V. (2002). Reentry in heterogeneous cardiac tissue described by the Luo-Rudy ventricular action potential model, *American Journal of Physiology Heart Circulation Physiology* 284: H542–H548.

Vigmond, E. J., Ruckdeschel, R. & Trayanova, N. (2001). Reentry in a morphologically realistic atrial model, *Journal of Cardiovascular Electrophysiology* 12(9): 1046–1054.

Virag, N., Jacquemet, V., Henriquez, C. S., Zozor, S., Blanc, O., Vesin, J.-M., Pruvot, E. & Kappenberger, L. (2002). Study of atrial arrhythmias in a computer model based on magnetic resonance images of human atria, *Chaos: An Interdisciplinary Journal of Nonlinear Science* 12: 754–763.

Wieser, L., Fischer, G., Nowak, C. & Tilg, B. (2007). Fibrillatory conduction in branching atrial tissue–Insight from volumetric and monolayer computer models, *Computer Methods and Programs in Biomedicine* 86: 103–111.

Wieser, L., Nowak, C., Tilg, B. & Fischer, G. (2008). Mother rotor anchoring in branching tissue with heterogeneous membrane properties, *Biomedizinische Technik* 53: 25–35.

Wieser, L., Richter, H., Plank, G., Pfeifer, B., Tilg, B., Nowak, C. & Fischer, G. (2008). A finite element formulation for atrial tissue monolayer, *Methods of Information in Medicine* 47: 131–139.

Wijffels, M., Kirchhof, C., Dorland, R. & Alessie (1995). Atrial fibrillation begets atrial fibrillation: a study in awake chronically instrumented goats, *Circulation* 92: 1954–1968.

Xie, F., Qu, Z., Garfinkel, A. & Weiss, J. (2002). Electrical refractory period restitution and spiral wave reentry in simulated cardiac tissue, *American Journal of Physiology Heart Circulation Physiology* 283: H448–H460.

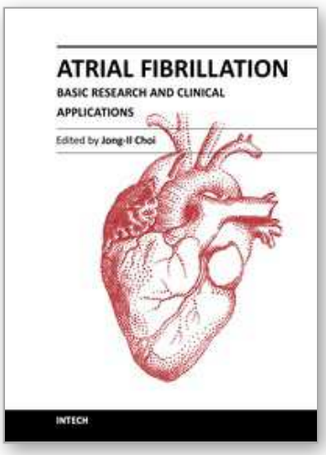

Atrial Fibrillation - Basic Research and Clinical Applications

Edited by Prof. Jong-Il Choi

ISBN 978-953-307-399-6
Hard cover, 414 pages
Publisher InTech
Published online 11, January, 2012
Published in print edition January, 2012

Atrial Fibrillation-Basic Research and Clinical Applications is designed to provide a comprehensive review and to introduce outstanding and novel researches. This book contains 22 polished chapters and consists of five sections: 1. Basic mechanisms of initiation and maintenance of atrial fibrillation and its pathophysiology, 2. Mapping of atrial fibrillation and novel methods of signal detection. 3. Clinical prognostic predictors of atrial fibrillation and remodeling, 4. Systemic reviews of catheter-based/surgical treatment and novel targets for treatment of atrial fibrillation and 5. Atrial fibrillation in specific conditions and its complications. Each chapter updates the knowledge of atrial fibrillation, providing state-of-the art for not only scientists and clinicians who are interested in electrophysiology, but also general cardiologists.

InTech Europe
University Campus STeP Ri
Slavka Krautzeka 83/A
51000 Rijeka, Croatia
Phone: +385 (51) 770 447
Fax: +385 (51) 686 166
www.intechopen.com

InTech China
Unit 405, Office Block, Hotel Equatorial Shanghai
No.65, Yan An Road (West), Shanghai, 200040, China
中国上海市延安西路65号上海国际贵都大饭店办公楼405单元
Phone: +86-21-62489820
Fax: +86-21-62489821

IntechOpen